# 100–300 GHz Gunn Oscillator Simulation Through Harmonic Balance Circuit Analysis Linked to a Hydrodynamic Device Simulator

M. F. Zybura, S. H. Jones, *Member, IEEE*, G. B. Tait, *Member, IEEE*, and J. R. Jones

*Abstract*— Accurate and efficient calculations of the large-signal AC behavior of second-harmonic InP Transferred Electron Oscillators (TEO's) are presented. This is accomplished by combining a novel harmonic balance circuit analysis technique with a hydrodynamic device simulator employing the temperature dependent drift and diffusion equations. The electron transport simulations include a detailed heat flow analysis to update the temperature profile in the device. The nonlinear circuit analysis utilizes a fixed-point iterative method derived from the robust multiple reflection algorithm. To expedite the process and aid in convergence, an acceleration technique is also employed in this algorithm. The associated reduction in computation time allows for the inclusion of a hydrodynamic treatment of the Transferred Electron Device (TED) using the modified drift and diffusion equations. Comparisons are made with the published experimental data reported by Rydberg on second-harmonic 188 GHz InP TEO's.

## I. INTRODUCTION

**R**YDBERG [1] has demonstrated as much as 7 mW of power at 188 GHz using second-harmonic InP devices, and recently Crowley *et al.* [2] has obtained 65 mW at 138 GHz. To optimize future harmonic device designs for increased power and higher frequencies, a design tool that efficiently determines power at all harmonics, as a function of the device characteristics, embedding circuit, and packaging parameters is required. Presently, computer-aided design programs are available for microwave nonlinear circuit analysis based on the harmonic balance numerical technique [3]. These codes reduce the nonlinear semiconductor devices to equivalent circuit elements with closed form analytical approximations for the current-voltage and capacitance-voltage characteristics, making the nonlinear circuit analysis possible. This approach is powerful for lower-frequency design and has been a critical factor in the design of integrated microwave circuits. For more complex and higher frequency millimeter wave circuits, however, the approximate equivalent circuit technique is not sufficiently accurate. In this work, an efficient fixed point iteration method derived from the multiple reflection technique [3] is employed facilitating the use of a hydrodynamic device

simulator using the drift and diffusion equations. The drift and diffusion equations utilize both field (0.1–100 kV/cm) and temperature (300–500 K) dependent mobility and diffusivity derived from Monte Carlo simulations and a thermal analysis that includes all regions of the device. Every aspect of the linked nonlinear circuit/ hydrodynamic device simulator has been designed for accuracy, computational speed, and robust convergence properties.

## II. DEVICE SIMULATOR

The device simulator employed here is a modified version of a previously described simulation program [4], [5]. The phenomenological hydrodynamic equations governing the physical model are the one-dimensional modified drift and diffusion equations and Poisson's equation,

$$\frac{\partial n}{\partial t} = \frac{1}{q}\frac{\partial J}{\partial x} \tag{1}$$

$$J = qnE\mu(E,T) + qD(E,T)\frac{\partial n}{\partial x} + qnD_n^T\frac{\partial T}{\partial x}, \tag{2}$$

and

$$\frac{\partial^2 \phi}{\partial x^2} = -\frac{q}{\epsilon}(N_D(x) - n), \tag{3}$$

where $n, q$, and $J$ are the electric charge density, the electron charge, and the particle current density, respectively. In (2), $E$, $\mu$, $D$, $D_n^T$, and $T$ are the electric field, the temperature and field dependent mobility and diffusivity, the thermal diffusivity, and the electron temperature, assumed to be the lattice temperature, respectively. In (3), $\phi$ is the scaler potential, $\epsilon$ is the dielectric permittivity of the device material, and $N_D(x)$ is the donor impurity concentration. The electric field is calculated from Poisson's equation, and the thermal gradient, $\partial T/\partial x$, is analytically determined from the thermal analysis described below.

The GaAs and InP electric field and temperature dependent mobility, $\mu(E,T)$, and diffusivity, $D(E,T)$, were calculated from three-valley Monte Carlo simulations. These simulations were performed using 10,000 superparticles at 50-degree increments from 300 to 500 K with a uniform donor concentration of $10^{16}\text{cm}^{-3}$. The Monte Carlo code is similar to the code used in [6], however to account for high temperature effects, along with lattice temperature, several material parameters were modified to be temperature dependent [7], [8]. Some

of these changes include the energy gaps and conduction valley minima separation of $\Gamma$, $L$. and $X$ valleys and the gamma valley electron effective mass. Both the mobility and diffusivity data has been numerically fit using equation (6-2-8) of reference [9], and the accompanying fit parameters are again fit versus temperature yielding surface contours for both mobility and diffusivity versus electric field and temperature. The above drift and diffusion transport equations form a set of coupled nonlinear partial differential equations, which are solved by the half-implicit Crank Nicolson finite difference scheme. Spatial and temporal increments typically are on the order of the length and time over which charge imbalances grow or decay. This technique offers substantial reductions in CPU time while retaining some important hot electron effects since $\mu(E, T)$ and $D(E, T)$ have been extracted from prior Monte Carlo analysis.

The thermal analysis described in reference [4] is performed in series with the drift and diffusion analysis. Closed form expressions for the temperature and temperature gradient are used in each layer of the packaged device given the layer dimensions, the ohmic contact resistance, and the power dissipated per unit volume $(Q)$ in that layer. $Q$ is determined from the aforementioned large signal ac numerical calculation of the device current and power. The frequency-dependent parasitic resistances of the device (DC-$n^{\text{th}}$ harmonic) are also calculated [10] and added to the respective embedding impedances also included in the nonlinear circuit analysis described below.

## III. HARMONIC BALANCE

To fully design transferred electron oscillators (TEO's), equal design consideration must be given to both the device and the circuit in which it is mounted. With a hydrodynamic device simulator, one can determine the optimal embedding impedances of the cavity presented to the device by optimizing the power generation as a function of the ac voltage. However, such an optimization is virtually impossible when considering higher harmonic components of the driving voltage. Similarly, finding a device design that has some pre-specified operating impedance is difficult when considering second- or third-harmonic operation. By linking both the device and circuit simulators, this problem can be overcome. The harmonic balance nonlinear circuit analysis technique employed here is an extension of the Siegel and Kerr multiple reflection algorithm [3]. The time-domain current through the device is calculated by the numerical device simulator for one period, as described in the previous section. The harmonic components of the current are extracted from the time-domain current waveform using a discrete fourier transform. A fixed-point iterative expression, derived from the multiple-reflection algorithm, is then used to update the total voltage applied directly across the device in terms of the circuit embedding impedances, the harmonic components of the current, and the harmonic components of the voltage from the previous iteration. This iterative process continues until the harmonic components of the voltage converge to their steady-state values.

The novelty in the harmonic balance algorithm utilized here is that, in deriving the fixed point iterative voltage update expression, we use *a priori* knowledge (from Kirchhoff's voltage law) that the nonlinear device impedance will equal the negative of the linear circuit impedance for each undriven harmonic in steady state $(Z_n^{NL} = -Z_n^L, n = 2, 3, \ldots, 6)$. This eliminates the computationally intensive and possibly unstable Runge-Kutta numerical integration necessary in the multiple-reflection technique and automatically calculates the complex under-relaxation parameters for each harmonic component of the fixed point update equation. Included with the fixed-point iteration is a Steffenson acceleration scheme adopted from the secant methods of numerical analysis [11]. Unlike Newton techniques, the difficult and time consuming numerical calculations needed for the assembly of Jacobian matrices and the solutions of large linear systems of equations are avoided, while maintaining a convergence rate nearly that of Newton-type methods.

## IV. RESULTS AND DISCUSSION

The algorithm by which the TEO simulations are performed is straightforward. The operating frequency, DC bias, circuit embedding impedances ($2^{\text{nd}} - 6^{\text{th}}$ harmonic), doping profile, and chip characteristics are adjustable inputs. The ac driving voltage, $V_1$, is allowed to sweep over a given range where optimal power, stability, and sufficient device impedances at the fundamental are anticipated. This limits the optimization to the dc and fundamental driving voltages. After each fixed-point iterative update of the voltage, the device current is numerically calculated using the drift and diffusion analysis, and the circuit and device impedances at each harmonic are tested for convergence $(Z_n^{\text{dev}} = -Z_n^{\text{ckt}}, n = 2, 3, \ldots, 6)$. Outputs include current and voltage waveforms, electric field and electron concentration profiles versus time and position, the temperature profile, and output power (DC-$6^{\text{th}}$ harmonic). In order to demonstrate the correlation between simulation and experimental results, comparisons have been made with published experimental data of Rydberg [1]. The InP device simulated and described in [1] has a 1.1-$\mu$m graded active region from $1.4 \times 10^{16}$ cm$^{-3}$ at the cathode to $1.6 \times 10^{16}$ cm$^{-3}$ at the anode and a 50 $\mu$m mesa diameter. At a fundamental frequency of 94 GHz and dc bias of 4 V, the simulations indicate peak power and stability for an impressed 2-V ac signal directly across the device. This gives a device impedance at the fundamental of $Z_1^{\text{dev}} = -0.8 - j6.6$ $\Omega$. Fig. 1 shows the resultant power versus circuit impedance surface contour for a domain of second harmonic (188 GHz) circuit impedances ranging from 1.80 $\Omega \leq R_2^{\text{ckt}} \leq 10.80$ $\Omega$ and 0 $\Omega \leq X_2^{\text{ckt}} \leq$ 10.0 $\Omega$. Because the device is typically capacitive, only positive reactances are considered. Six harmonics are considered, and in this case the embedding impedances of the higher harmonics ($3^{\text{rd}} - 6^{\text{th}}$) are set to 0.001$\Omega$ for both resistive and reactive components. The frequency dependent parasitic resistances are added to the corresponding linear embedding impedances. Peak performance of 6.4 mW is predicted for a second harmonic circuit impedance, $Z_2^{\text{ckt}} \approx 2.3 + /j3.0\Omega$. Power generation greater than 1.5 mW is expected for circuit
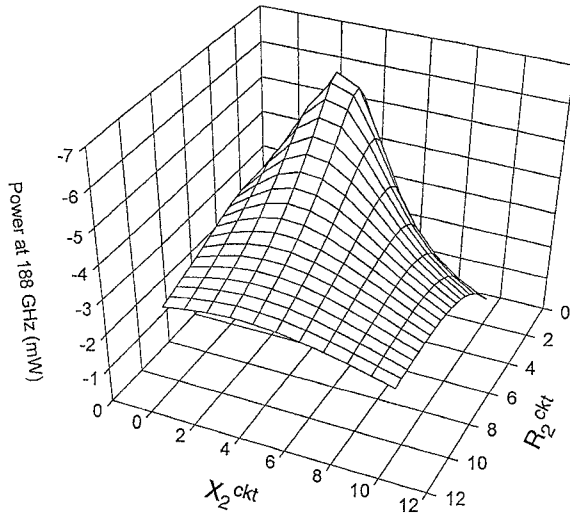
Fig. 1. Second harmonic (188 GHz) power versus second harmonic circuit impedances for the device of [1] with $V_{DC} = 4.0$V, $V_{ac} = 2.0$V, and $Z_1^{ckt} = 0.8 + j6.6$ $\Omega$. Higher harmonic ($n \geq 3$) resistive and reactive components are set to 0.001 $\Omega$ plus the series resistance of the chip.

offered, simulations compare favorably for second-harmonic performance. Recent work by Jones *et al.* [12] has shown dramatic increases in the second- and third-harmonic current waveform content associated with doping mesas placed in the device active region. The potential increase in output power for 200–300 GHz second harmonic InP TEO's is expected for longer, higher impedance devices and is presently being researched. Also, increases in third-harmonic power using a modulated doping profile in the device active region are expected and are being explored.

## ACKNOWLEDGMENT

impedances as large as $Z_2^{ckt} = 10.8 + j10$. Experimentally, Rydberg has demonstrated $\approx 7$ mW of power generated at 188 GHz in second-harmonic operation. Similar simulations have been performed for third-harmonic operation (282 GHz) using the stable second harmonic operating impedance $Z_2^{ckt} = 2.0 + j3.5$ $\Omega$. The anticipated output power varies from $\approx .1 - 1.5$ mW over a range of third-harmonic circuit impedances $1.67$ $\Omega \leq R_3^{ckt} \leq 10.67$ $\Omega, 0$ $\Omega \leq X_3^{ckt} \leq 10$ $\Omega$.

## V. CONCLUSION

The interaction between device and circuit is critical to high frequency TEO performance. With this CAD tool, efficient design of second- and third-harmonic TEO's is possible. Typical convergence time for a given operating point involves about ten harmonic balance iterations and a total wall time of under a minute on a Hewlett Packard 735 workstation. Although specific circuit embedding impedances are unavailable for Rydberg's cavity over the range of impedances

## REFERENCES

[1] A. Rydberg, "High efficiency and output power from second- and third-harmonic millimeter wave InP-TED oscillators at frequencies above 170 GHz," *IEEE Electron Device Lett.* , vol. 11, no. 10, pp. 439–441, 1990.
[2] J. D. Crowley, C. Hang, R. E. Dalrymple, D. R. Tringali, F. B. Fank, L. Wandinger, and H. B. Wallace, "140 GHz indium phosphide Gunn diode," *Electronics Lett.*, vol. 30, no. 6, pp. 499–500, 1994.
[3] P. H. Siegel, A. R. Kerr, and W. Hwang, "Topics in the optimization of millimeter-wave mixers," NASA Tech. Papers, No. 2287, Mar. 1984.
[4] M. F. Zybura, S. H. Jones, and G. B. Tait, "Efficient computer aided design of second-harmonic GaAs and InP millimeter wave TEDs," in *Proc. Int. Semiconductor Device Res. Symp.*, 1993, vol. 2, pp. 775–778.
[5] G. B. Tait and C. M. Krowne, "Efficient transferred electron device simulation method for microwave and millimeter wave CAD applications," *Solid-St. Electron.*, vol. 30, no. 10, pp. 1025–1036, 1987.
[6] G. U. Jensen, B. Lund, T. A. Fjeldly, and M. Shur, "Monte Carlo simulation of semiconductor devices," *Comp. Phys. Comm.* , vol. 6, pp. 1–61, 1991.
[7] J. S. Blakemore, "Semiconducting and other major properties of GaAs," *J. Appl. Phys.* vol. 53, pp. R123–R181, 1982.
[8] O. Madelung, Ed., *Semiconductors, Group IV Elements and III-V Compounds*. Heidelberg, Germany: Springer-Verlag, 1991.
[9] M. Shur, *Physics of Semiconductor Devices.*, Englewood Cliffs, NJ: Prentice-Hall, 1990.
[10] S. A. Maas, *Nonlinear Microwave Circuits.* Norwood, MA: Artech House, 1988, Ch. 2, pp. 49–51.
[11] J. Ortega and W. Rheinboldt, *Iterative Solution of Nonlinear Equations in Several Variables.* New York: Academic Press, 1970.
[12] S. H. Jones, G. B. Tait, and M. Shur, "Modulated-impurity- concentration transferred electron devices exhibiting large harmonic frequency content," *Microwave and Opt. Tech. Lett.*, vol. 5, no. 8, pp. 354–359, 1992.